

# Interactions of fractional solitons with local defects: Stabilization and scattering

Thawatchai Mayteevarunyoo<sup>1</sup> and Boris A. Malomed<sup>2,3</sup>

<sup>1</sup>*Department of Electrical and Computer Engineering,  
Faculty of Engineering, Naresuan University, Phitsanulok 65000, Thailand*

<sup>2</sup>*Department of Physical Electronics, School of Electrical Engineering,  
Faculty of Engineering, Tel Aviv University, P.O.B. 39040, Ramat Aviv, Tel Aviv, Israel and*

<sup>3</sup>*Instituto de Alta Investigación, Universidad de Tarapacá, Casilla 7D, Arica, Chile*

Stability is an essential problem in theoretical and experimental studies of solitons in nonlinear media with fractional diffraction, which is represented by the Riesz derivative with Lévy index (LI)  $\alpha$ , taking values  $\alpha < 2$ . Fractional solitons are unstable at  $\alpha \leq 1$  or  $\alpha \leq 2$  in uniform one-dimensional media with the cubic or quintic self-focusing, respectively. We demonstrate that, in these cases, the solitons may be effectively stabilized by pinning to a delta-functional trapping potential (attractive defect), which is a relevant setting in optical waveguides with the effective fractional diffraction. Using the respective fractional nonlinear Schrödinger equation with the delta-functional potential term, we find that, in the case of the cubic self-focusing, the fractional solitons are fully stabilized by the pinning to the defect for  $\alpha = 1$ , and partly stabilized for  $\alpha < 1$ . In the case of the quintic self-focusing, the full and partial stabilization are found for  $\alpha = 2$  and  $\alpha < 2$ , respectively. In both cases, the instability boundary is exactly predicted by the Vakhitov-Kolokolov criterion. Unstable solitons spontaneously transform into oscillating breathers. A variational approximation (VA) is elaborated parallel the numerical analysis, with a conclusion that the VA produces accurate results for lower LI values, i.e., stronger fractionality. In the cubic medium, collisions of traveling stable solitons with repulsive and attractive defects are addressed too, demonstrating outcomes in the form of rebound, splitting, and passage.

The consideration of linear and nonlinear systems with effective fractional diffraction and/or dispersion is one of basic directions in the development and investigation of complexity in various fields of physics, such as optics, quantum matter, solid state, classical field theory, and others. While the fractional calculus was known, as a mathematical curiosity, in the course of the past 200 years, the concept of fractional dispersion had been introduced in physics, in the form of fractional quantum mechanics, by N. Laskin, in 2000. In this context, the commonly known one-dimensional (1D) operator of the kinetic energy,  $-d^2/dx^2$ , is replaced by the fractional-order *Riesz derivative*,  $(-d^2/dx^2)^{\alpha/2}$ , with the *Lévy index* (LI)  $\alpha$ , so that the canonical (non-fractional) theory corresponds to  $\alpha = 2$ , while the fractality corresponds to  $\alpha < 2$ . With all its theoretical appeal, fractional quantum mechanics remains far from experimental realization. To advance the fractality concept to other branches of physics, and push it closer to a possibility of experimental implementation, it was proposed by S. Longhi in 2015, using the commonly known similarity between the quantum-mechanical Schrödinger equation and the parabolic equation for the classical paraxial propagation (diffraction) of light, to emulate fractional quantum mechanics by effective fractional diffraction in optical cavities. Only in 2023, the first experimental realization of fractional optics was reported, in terms of the light transmission in optical fiber cavities which feature effective fractional dispersion. While the first theoretical and experimental implementations of the fractional light propagation were reported in the linear form, the intrinsic nonlinearity of optical materials suggest a possibility of consideration of nonlinear modes, such as fractional solitons, supported by the interplay of the fractional diffraction/dispersion and material nonlinearity. This possibility was recently elaborated in many theoretical works. The first experimental demonstration of fractional temporal solitons in fiber cavities was reported very recently [14, 15]. In this context, the stability of fractional solitons is a crucially important issue. In particular, in the 1D space, the interplay of the usual Kerr (cubic) self-focusing with the fractional diffraction gives rise to stable solitons in the interval of  $1 < \alpha \leq 2$ , while they are unstable, because of the occurrence of the *critical* and *supercritical* collapse, at  $\alpha = 1$  and  $\alpha < 1$ , respectively. In the case of the quintic self-focusing, which is also possible in optical materials, fractional solitons are unstable at all values of  $\alpha \leq 2$ . Therefore, stabilization of fractional solitons is an issue of major significance. The present paper demonstrates that the stabilization may be provided by using a linear potential in the form of a local potential well (attractive local defect). By means of a systematic numerical investigation and an analytical variational approximation, combined with the well-known *Vakhitov-Kolokolov criterion*, it is demonstrated that, in the case of the cubic self-focusing, the fractional solitons, pinned to the attractive defect, are completely and partly stabilized for  $\alpha = 1$  and  $\alpha < 1$ , respectively. Similarly, in the case of the quintic self-focusing, the complete and partial stabilization of the pinned solitons is demonstrated for  $\alpha = 2$  and  $\alpha < 2$ , respectively.

## I. INTRODUCTION AND THE MODEL

In the course of the past two decades, models based on linear and nonlinear Schrödinger equations with fractional dispersion, and similar equations with fractional operators, have drawn much interest in physical kinetics [1, 2], quantum theory [3–6],

and optics [7], see also reviews [8, 9]. The first experimental realization of the linear Schrödinger equation with the effective fractional group-velocity dispersion was performed in fiber-laser cavities operating in the linear regime [10]. The interplay of the fractional dispersion and intrinsic nonlinearity of optical materials gives rise to fractional nonlinear Schrödinger equations (FNLSEs), which produce various solutions in the form of fractional solitons [11–13]. Very recently, fiber optics was employed to demonstrate the creation of such solitons in the temporal domain [14, 15].

The one-dimensional (1D) FNLSE is introduced, in the scaled form, as

$$i \frac{\partial \psi}{\partial z} = \frac{1}{2} \left( -\frac{\partial^2}{\partial x^2} \right)^{\alpha/2} \psi - N(|\psi|^2) \psi + U(x) \psi, \quad (1)$$

It is written in the notation adopted for the propagation of optical waves, with complex amplitude  $\psi(x, z)$ , in the spatial domain spanned by the propagation distance  $z$  and transverse coordinate  $x$ . The equation may include an effective real potential  $U(x) \sim -\delta n(x)$ , where  $\delta n(x)$  is a local change of the refractive index. Term  $N(|\psi|^2) \psi$  in Eq. (1), with  $N(|\psi|^2) > 0$ , represents the self-focusing nonlinearity, in the general form

The fractional-diffraction operator in Eq. (1), with Lévy-index (LI)  $\alpha \leq 2$  [16], is represented by the Riesz derivative [17]. Unlike abstract concepts of fractional derivatives, such as the Caputo operator [18], the definition of the Riesz derivative is based on the natural idea that, in the Fourier space with wavenumber  $p$ , which is dual to coordinate  $x$ , the fractional differentiation amounts to the multiplication by  $|p|^\alpha$ . This idea leads to the definition based on the cascaded direct and inverse Fourier transforms:

$$\left( -\frac{\partial^2}{\partial x^2} \right)^{\alpha/2} \psi \equiv D_{\text{Riesz}}^{(\alpha)} = \frac{1}{2\pi} \int_{-\infty}^{+\infty} dp |p|^\alpha \int_{-\infty}^{+\infty} d\tilde{x} \exp(ik(x-\tilde{x})) \psi(\tilde{x}). \quad (2)$$

Thus, the Riesz derivative is actually an integral operator, rather than a differential one. In the limit case of  $\alpha = 2$  it carries over to the usual second derivative,  $D_{\text{Riesz}}^{(\alpha=2)} = -\frac{\partial^2}{\partial x^2}$ .

In the free space ( $U(x) = 0$ ), the self-focusing nonlinearity in Eq. (1) gives rise to a family of fractional solitons with real propagation constant  $k > 0$  and real function  $u(x)$ ,

$$\psi(x, z) = e^{ikz} u(x). \quad (3)$$

The soliton is characterized by its power,

$$P = \int_{-\infty}^{+\infty} [u(x)]^2 dx. \quad (4)$$

In the case of the power-law nonlinear term,

$$N(|\psi|^2) = |\psi|^{2\sigma}, \quad (5)$$

the scaling properties of Eq. (1) in the free space ( $U(x) = 0$ ) predict the following dependence between the propagation constant and power:

$$P \sim k^{(\alpha-\sigma)/(\alpha\sigma)}. \quad (6)$$

The soliton solutions of the non-fractional NLSE ( $\alpha = 2$ ) with the general form (5) of the power-law nonlinearity can be easily found in the exact form,

$$u(x) = \left[ \sqrt{(\sigma+1)k} \operatorname{sech}(\sigma\sqrt{2kx}) \right]^{1/\sigma}. \quad (7)$$

The integral power (4) of solitons (7) is

$$P_{\alpha=2,\sigma}(k) = \sqrt{\frac{\pi}{2}} \frac{(\sigma+1)^{1/\sigma} \Gamma(1/\sigma)}{\sigma \Gamma((2+\sigma)/(2\sigma))} k^{(2-\sigma)/(2\sigma)} \quad (8)$$

[24], cf. Eq. (6), where  $\Gamma$  is the Euler's Gamma-function.

If LI is not too low, *viz.*,  $\alpha > \sigma$ , relations (6) and (8) (the latter one corresponds to  $\alpha = 2$ ) satisfy the celebrated Vakhitov-Kolokolov (VK) criterion [19–21],  $dP/dk > 0$ , which is the necessary (although not sufficient) stability condition of the soliton family. In the case of  $\alpha \leq \sigma$ , when the family does not satisfy the VK criterion, the instability may initiate the onset of the *critical* and *supercritical* collapse (spontaneous blowup leading to the emergence of singular states) in the cases of  $\alpha = \sigma$  and

$\alpha < \sigma$ , respectively [9, 22]. In the former case, the corresponding family of unstable *Townes solitons* (TSs) is degenerate, in the sense that its power takes a single value which does not depend on  $k$ , in accordance with Eq. (6). In particular, for the non-fractional ( $\alpha = 2$ ) NLSE with the quintic self-focusing term ( $\sigma = 2$  in Eq. (5)), Eq. (7) produces the commonly known family of 1D TS solutions [23]. The single value of power (4) for this TS family is given by Eq. (8) with  $\alpha = 0$ :

$$P_{\text{TS}}^{(\alpha=\sigma=2)} = \sqrt{\frac{3}{2}} \frac{\pi}{2} \approx 1.92. \quad (9)$$

For the realization in optics, most relevant is the Kerr (cubic) nonlinearity, corresponding to  $\sigma = 1$  in Eq. (5). The cases of the quintic and septimal nonlinearities, which correspond to  $\sigma = 2$  and 3, respectively, are relevant too, as they can be experimentally realized in the light propagation in colloidal suspensions of metallic nanoparticles [25, 26].

In this connection, it is relevant to mention that LI values  $\alpha \leq 1$  were not considered in a majority of theoretical studies dealing with FNLSEs precisely for the reason that they give rise to the collapse in the combination with the Kerr nonlinearity. Nevertheless, the methods proposed for the creation of the effective fractional diffraction [7] and dispersion [10] are as appropriate for  $\alpha \leq 1$  as they are for  $\alpha > 1$ .

Thus, the stability of fractional solitons is an essential problem, which has drawn considerable interest. In particular, a possibility for the creation and stabilization of fractional solitons under the action of spatially periodic (lattice) potentials was elaborated in various forms

A possibility to create stable solitons in the 1D medium with the usual (non-fractional) diffraction,  $\alpha = 2$ , and the self-focusing nonlinearity (5) with  $\sigma \geq 2$ , when the solitons in the uniform medium are unstable, according to the VK criterion, was proposed in Ref. [24], by means of the delta-functional attractive potential, which corresponds to

$$U(x) = -\varepsilon \delta(x), \quad (10)$$

in Eq. (1), with  $\varepsilon > 0$ . In optics, this potential represents a narrow strip in the planar waveguide with a large refractive index.

Exact solutions for solitons pinned to the delta-functional attractive center (alias *attractive defect*) are given by Eq. (7), with replacement

$$x \rightarrow (|x| + \Xi), \quad \Xi = \left(2\sigma\sqrt{2k}\right)^{-1} \ln \left( \frac{\sqrt{2k} + \varepsilon}{\sqrt{2k} - \varepsilon} \right). \quad (11)$$

As seen from Eq. (11), the pinned solitons exist with values of the propagation constant  $k \geq k_{\min} = \varepsilon^2/2$  ( $k_{\min}$  is the eigenvalue for the bound state produced by the linear equation with the non-fractional diffraction,  $\alpha = 2$ ). Both the VK criterion and full numerical analysis [24] demonstrate that the pinned solitons are fully stable in the semi-infinite interval of  $k_{\min} \leq k < \infty$ , for the critical quintic nonlinearity,  $\sigma = 2$ , and in a finite interval,  $k_{\min} \leq k \leq k_{\max}$ , for  $\sigma > 2$ . In particular,  $k_{\max} \approx 8\varepsilon^2/[\pi(\sigma - 2)]^2$  for  $0 < \sigma - 2 \ll 1$  [24].

The objective of this work is to introduce the FNLSE model with the nonlinearity (5) and delta-functional potential (10):

$$i \frac{\partial \psi}{\partial z} = \frac{1}{2} \left( -\frac{\partial^2}{\partial x^2} \right)^{\alpha/2} \psi - |\psi|^{2\sigma} \psi - \varepsilon \delta(x) \psi, \quad (12)$$

and analyze a possibility of the stabilization of fractional solitons pinned to the attractive defect in the relevant cases, corresponding to  $\alpha \leq 1$  with the cubic self-focusing ( $\sigma = 1$ ), and  $\alpha < 2$  with the quintic self-focusing ( $\sigma = 2$ ), when the solitons are completely unstable in the free space ( $U = 0$ ). As mentioned above, these settings can be implemented in fractional nonlinear optical waveguides, and may find applications in various soliton-based data-processing schemes [31].

The substitution of ansatz (3) in Eq. (12) leads to the real stationary equation:

$$ku + \frac{1}{2} \left( -\frac{d^2}{dx^2} \right)^{\alpha/2} u - u^{2\sigma+1} - \varepsilon \delta(x) u = 0. \quad (13)$$

By means of rescaling, we set  $\varepsilon \equiv 1$  in Eqs. (12) and (13) for  $\alpha \neq 1$ , while  $\varepsilon$  should be kept as a free parameter in the special case of  $\alpha = 1$ .

The subsequent presentation is arranged as follows. Making use of the possibility to represent Eq. (13) in the Lagrangian form [9, 22, 32], the variational approximation (VA) for the fractional solitons pinned to the attractive defect is developed in Section 2. Numerical results for families of the pinned solitons, including the analysis of their stability, are collected and compared to predictions of VA in Section 3. In addition, collisions of traveling stable fractional solitons with the local defect, attractive or repulsive (the latter one corresponds to  $\varepsilon < 0$  in Eq. (10)), in the case of  $\sigma = 1$  (the cubic self-focusing) and  $\alpha > 1$ , are considered in Section 4. In the same section, we briefly consider symmetric two-soliton bound states attached to the repulsive defect, concluding that such states exist but are unstable against spontaneous symmetry-breaking splitting. The paper is concluded by Section 5.

## II. THE VARIATIONAL APPROXIMATION (VA)

The variational and numerical results are produced below with the ideal delta-function in Eqs. (12) and (13) replaced by its standard Gaussian regularization,

$$\tilde{\delta}(x) = (\sqrt{\pi}\xi)^{-1} \exp\left(-\frac{x^2}{\xi^2}\right). \quad (14)$$

The delta-function limit (10) for the potential is valid if the regularization scale  $\xi$  in approximation (14) is much smaller than the inner scale of the soliton, which may be estimated as  $\sim k^{-1/\alpha}$  (cf. Eq. (6)), i.e., under the condition of  $\xi \ll k^{-1/\alpha}$ . The numerical results are presented below for  $\xi = 0.05$ , which satisfies the latter condition for relevant cases.

Taking into regard definitions (2) of the Riesz derivative and regularized delta-function (14), Eq. (13) can be derived from the following Lagrangian:

$$L = \frac{k}{2} \int_{-\infty}^{+\infty} dx [u(x)]^2 + \frac{1}{8\pi} \int_{-\infty}^{+\infty} dp |p|^\alpha \int_{-\infty}^{+\infty} dx \int_{-\infty}^{+\infty} d\bar{x} \exp(ip(x-\bar{x})) u(x) u(\bar{x}) - \frac{1}{2(\sigma+1)} \int_{-\infty}^{+\infty} dx [u(x)]^{2(\sigma+1)} - \frac{\varepsilon}{2\sqrt{\pi}\xi} \int_{-\infty}^{+\infty} dx \exp\left(-\frac{x^2}{\xi^2}\right) [u(x)]^2. \quad (15)$$

An analytically tractable version of VA is based on the Gaussian ansatz with amplitude  $A$  and width  $W$ :

$$u(x) = A \exp\left(-\frac{x^2}{2W^2}\right), \quad (16)$$

the respective power (21) being

$$P_{\text{VA}} = \sqrt{\pi} A^2 W. \quad (17)$$

The VA Lagrangian in the free space ( $\varepsilon = 0$ ) for  $\sigma = 1$ , produced by the substitution of ansatz (16) in Lagrangian (15), was known previously [9]. In the present case, which includes the potential term  $\sim \varepsilon$  and the general value of the nonlinearity degree  $\sigma$ , the result is

$$L_{\text{VA}} = \frac{k}{2} P_{\text{VA}} + \frac{\Gamma((1+\alpha)/2)}{4\sqrt{\pi}} \frac{P_{\text{VA}}}{W^\alpha} - \frac{(P_{\text{VA}})^{\sigma+1}}{2\pi^{\sigma/2}(\sigma+1)^{3/2}W^\sigma} - \frac{\varepsilon P_{\text{VA}}}{2\sqrt{\pi}\sqrt{W^2+\xi^2}}, \quad (18)$$

where  $\Gamma$  is the Gamma-function, and Eq. (17) was used to eliminate  $A^2$  in favor of  $P$ . Note that the last term in Eq. (18), which accounts for the effect of the attractive defect, carries over into  $\varepsilon P_{\text{VA}} / (2\sqrt{\pi}W)$  in the limit of  $\xi \rightarrow 0$ , which corresponds to the limit of the ideal delta-function in Eq. (14).

The variational (Euler-Lagrange) equations following from Lagrangian (18) are

$$\partial L_{\text{VA}} / \partial P_{\text{VA}} = \partial L_{\text{VA}} / \partial W = 0. \quad (19)$$

These equations make it possible to find, in the framework of VA, values of the propagation constant  $k$  and width  $W$  corresponding to given power  $P$ . Thus, the first equation in system (19) yields an expression for  $k$  in terms of  $P$  and  $W$ :

$$k = -\frac{\Gamma((1+\alpha)/2)}{2\sqrt{\pi}W^\alpha} + \frac{(P_{\text{VA}})^\sigma}{\pi^{\sigma/2}\sqrt{\sigma+1}W^\sigma} + \frac{\varepsilon}{\sqrt{\pi}\sqrt{W^2+\xi^2}}. \quad (20)$$

The second equation in system (19) gives rise to a relation which determines  $W$  for given  $P_{\text{VA}}$ :

$$(P_{\text{VA}})^\sigma = \frac{(\sigma+1)^{3/2}}{\sigma} \pi^{(\sigma-1)/2} \left[ \frac{\alpha}{2} \Gamma\left(\frac{\alpha+1}{2}\right) W^{\sigma-\alpha} - \varepsilon \frac{W^{\sigma+2}}{(W^2+\xi^2)^{3/2}} \right]. \quad (21)$$

In the absence of the attractive defect ( $\varepsilon = 0$ ), Eq. (21) demonstrates that, in the case of  $\alpha = \sigma$ , which gives rise to the TS family, the corresponding VA-predicted single value of the power (one that does not depend on  $k$ ) is

$$(P_{\text{VA}})_{\text{TS}}^{(\alpha=\sigma, \varepsilon=0)} = \frac{1}{2} (\sigma+1)^{3/2} \pi^{(\sigma-1)/2} \Gamma\left(\frac{\sigma+1}{2}\right). \quad (22)$$

In particular, Eq. (22) yields

$$(P_{\text{VA}})_{\text{TS}}^{(\alpha=\sigma=1, \varepsilon=0)} = \sqrt{2}, \quad (P_{\text{VA}})_{\text{TS}}^{(\alpha=\sigma=2, \varepsilon=0)} = \frac{1}{2} \sqrt{3\sqrt{3}\pi} \approx 2.02. \quad (23)$$

The comparison of the VA prediction, given by Eq. (23) for the power of the TS family with  $\alpha = \sigma = 2$ , and the exact value of the same power, as given by Eq. (9), demonstrates that the accuracy of the VA prediction is  $\approx 5\%$ .

As said above, the objective of the analysis is the possibility to stabilize the fractional soliton by the pinning it to the attractive defect, with  $\varepsilon > 0$ . This possibility can be further considered in the analytical form for the limit case of  $\xi = 0$  (the ideal delta-function in Eq. (13)), as the case of finite  $\xi$  is too cumbersome for the analytical study. Then, Eq. (21) is simplified to

$$(P_{\text{VA}})^\sigma = \frac{(\sigma+1)^{3/2}}{\sigma} \pi^{(\sigma-1)/2} \left[ \frac{\alpha}{2} \Gamma\left(\frac{\alpha+1}{2}\right) W^{\sigma-\alpha} - \varepsilon W^{\sigma-1} \right]. \quad (24)$$

The numerical results presented below in Fig. 2 suggest that the soliton pinned to the attractive defect exists with the power taking values below a certain maximum, which corresponds to  $dP_{\text{VA}}/dW = 0$ , in terms of the VA. As it follows from Eq. (24), the latter condition yields no result for  $\sigma = 1$ , while for  $\sigma = 2$  the maximum is attained at  $W = W_m$ , with

$$W_m^{\alpha-1} = \frac{1}{2} \alpha (2-\alpha) \Gamma\left(\frac{\alpha+1}{2}\right) \quad (25)$$

(here, as said above,  $\varepsilon \equiv 1$  is set). The substitution of value (25) in expression (24) with  $\sigma = 2$  and  $\varepsilon = 1$  yields the maximum value of the power, as a function of  $\alpha$ :

$$(P_{\text{max}})_{\text{VA}}^{(\sigma=2, \xi=0)}(\alpha) = \sqrt{\frac{3}{2} \sqrt{3\pi} (\alpha-1) \left( \frac{\alpha}{2} \Gamma\left(\frac{\alpha+1}{2}\right) \right)^{1/(1-\alpha)} (2-\alpha)^{(2-\alpha)/(\alpha-1)}}. \quad (26)$$

In particular, the limit value of this expression for  $\alpha \rightarrow 2$  is

$$(P_{\text{max}})_{\text{VA}}^{(\sigma=2, \xi=0)}(\alpha=2) = 3^{3/4} \approx 2.28. \quad (27)$$

Naturally, this value exceeds its counterpart (23) corresponding to  $\varepsilon = 0$ .

Further consideration demonstrates that Eq. (25) yields values which monotonously decrease from  $W_m = 1.2$  towards  $W_m = 0$  as LI decreases from  $\alpha = 1.5$  to  $\alpha = 0$ . This fact implies that, at  $\alpha < 1.5$ ,  $W_m$  is not large enough in comparison to the value  $\xi = 0.05$  adopted in Eq. (14), hence the simplified VA prediction (26), obtained by setting  $\xi = 0$  in Eq. (21), is not relevant for the comparison with numerical results at  $\alpha < 1.5$ .

### III. NUMERICAL RESULTS FOR SOLITONS PINNED TO THE ATTRACTIVE DEFECT

Numerical solutions of Eqs. (12) and (13), with the delta-function approximated by expression (14), were performed, chiefly, in the computational domain  $-8 < x < +8$ , discretized by  $2^{12}$  points. This domain size is sufficient, as it is much larger than the width of numerically found solitons, see Figs. 1 and 6 below. Stationary solutions were produced by means of the modified square operator method [33], with zero boundary conditions at  $x = \pm 8$ . Simulations of the evolution were run by means of the split-step Fourier method with longitudinal step  $\Delta z = 0.0001$ .

#### A. The case of the quintic self-focusing ( $\sigma = 2, \alpha < 2$ )

As mentioned above, the quintic nonlinearity ( $\sigma = 2$ ) makes all solitons unstable in the free space (with  $U = 0$ ) for all values of LI  $\alpha \leq 2$ , while the quasi-delta-functional potential  $U(x) = -\tilde{\delta}(x)$  (see Eq. (14)) may stabilize them. Typical examples of numerically found *stable* solitons pinned by the potential are displayed in Fig. 1, along with their VA-predicted counterparts, for a fixed propagation constant,  $k = 10$ , and LI values  $\alpha = 1.8, 1.5, 1.2$ , and  $1.05$ . It is seen that the VA, which is based on the numerical solution of the Euler-Lagrange equations (20) and (21), is quite accurate in these cases. The decrease of  $\alpha$  makes the effective diffraction weaker, hence the solitons become narrower.

The results for the existence and stability of the pinned solitons in this model are summarized in Fig. 2, in the form of dependences of the total power on the propagation constant,  $P(k)$ , for five LI values,  $\alpha = 2.0, 1.8, 1.5, 1.1$ , and  $0.8$  (the first one,  $\alpha = 2.0$ , pertains to the NLSE with the usual (non-fractional) diffraction, for which the full stability of the pinned solitons was demonstrated in Ref. [24]). A remarkable fact is that the stabilization remains valid, in a narrow interval of values of  $k$ , even

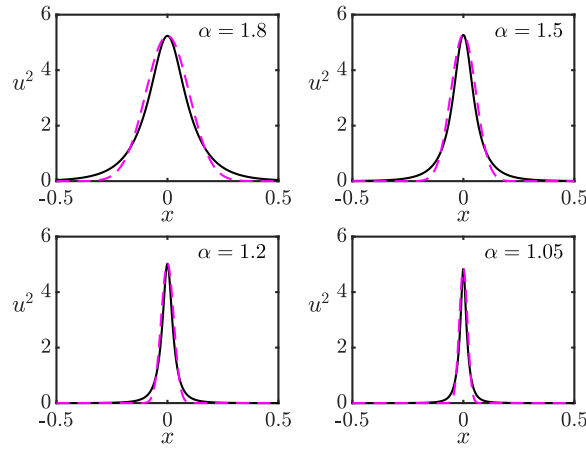


FIG. 1. Power profiles,  $(u(x))^2$ , of the numerically found and VA-predicted stable solitons are displayed by continuous black and dashed magenta lines, respectively, in the case of the quintic self-focusing ( $\sigma = 2$ ) and propagation constant  $k = 10$  in Eq. (13). The corresponding LI values  $\alpha$  are indicated in panels. The solitons are pinned to potential  $U(x) = -\delta(x)$ , see Eq. (14). The numerical results are produced as solutions of Eq. (13) with the delta-function approximated as per Eq. (14). The VA profiles are based on ansatz (16), with parameters obtained from the numerical solutions of Eqs. (20, (21) and (17).

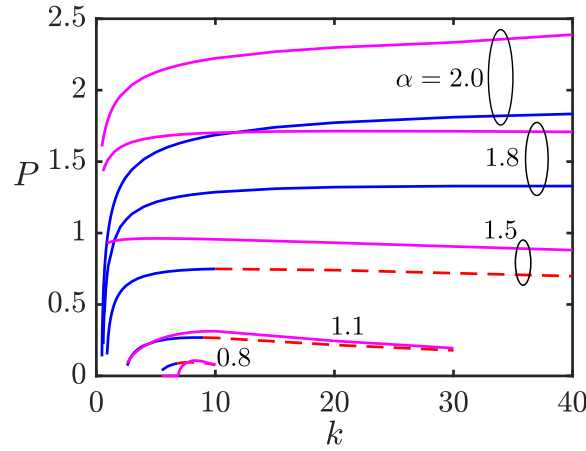


FIG. 2. The power,  $P$ , of families of the fractional solitons pinned by the attractive potential  $-\delta(x)$ , as produced by the numerical solution of Eq. (13), vs. the propagation constant,  $k$ , for the quintic nonlinearity ( $\sigma = 2$ ) and LI values  $\alpha$  indicated in the figure. Solid blue and dashed red lines denote stable and unstable solitons, respectively, the stability being identified by simulations of the perturbed propagation of the solitons in the framework of Eq. (12). The VA-predicted soliton families, produced by the numerical solution of Eqs. (20) and (21), are plotted by solid magenta lines.

for the value of LI as small as  $\alpha = 0.8$ , and the simple VA, based on the Gaussian ansatz (16), is quite accurate for low values of LI (which correspond to strong fractionality), *viz.*, for  $\alpha = 0.8$  and  $1.1$ , becoming less accurate for larger values of  $\alpha$ . It is also seen that the instability boundary, located at points with  $dP/dk = 0$ , precisely conforms to the VK criterion.

As mentioned above, both numerical and VA results demonstrate that, for given LI  $\alpha$ , the pinned solitons exist below a certain maximum value of the power,  $P < P_{\max}$ . The numerically found dependence  $P_{\max}(\alpha)$ , produced by Eq. (13) with  $\sigma = 2$ , is plotted in Fig. 3, along with its simplified-VA counterpart, as given by Eqs. (26) and (27).

When the pinned solitons are unstable, systematically performed simulations demonstrate that the instability does not lead to the collapse (blowup of the solution), which might be expected in the case when the solitons do not satisfy the VK criterion. Instead, the pinning potential still produces a stabilizing effect, which transforms the unstable stationary solitons into breathers featuring somewhat irregular inner oscillations, see a generic example in Fig. 4 (a similar trend was reported in Ref. [24] in the model with the non-fractional diffraction,  $\alpha = 2$ , and supercritical self-attraction, which corresponds to  $\sigma > 2$  in Eq. (12)).

The above results were obtained, as mentioned above, fixing  $\varepsilon = 1$  in Eqs. 12 and (13) by means of rescaling. It was mentioned too that the rescaling of  $\varepsilon$  is not possible in the case of  $\alpha = 1$ . In the latter case, the existence and stability of the numerically found pinned solitons are displayed in Fig. 5, by means of dependences  $P(\varepsilon)$  for three fixed values of the propagation constant,  $k = 5, 15$ , and  $30$ . It is observed that, quite naturally, the stability requires the action of a sufficiently strong pinning potential.

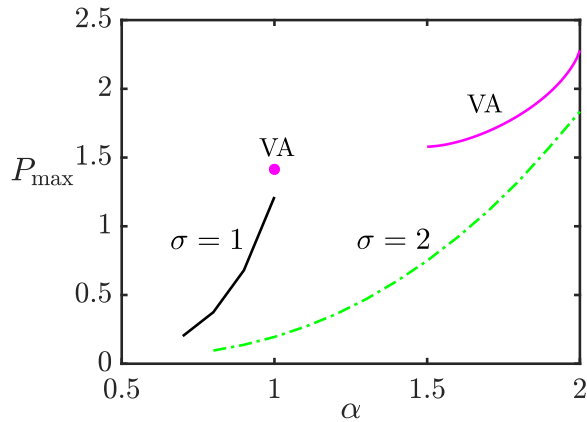


FIG. 3. The largest power  $P_{\max}$ , up to which the pinned solitons are produced by the numerical solution of Eq. (13), vs. LI  $\alpha$ . As indicated in the figure, the dependences  $P_{\max}(\alpha)$  are plotted for the cubic and quintic self-focusing ( $\sigma = 1$  and  $2$ , respectively). For  $\sigma = 2$ , the dependence predicted by the simplified VA (Eqs. (26) and (27)) is displayed by the magenta line (as explained in the text, it is irrelevant for  $\alpha < 1.5$ ). The magenta dot shows the largest value of  $P$  predicted by the VA for  $\sigma = 1$ , as per Eq. (23).

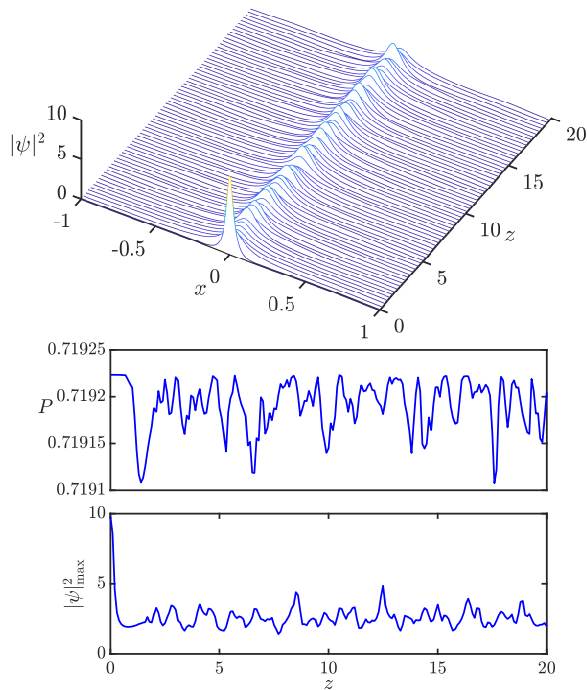


FIG. 4. The top panel: spontaneous transformation of an unstable pinned soliton, with propagation constant  $k = 30$ , into a breather, produced by simulations of Eq. (12) with  $\sigma = 2$  and  $\alpha = 1.5$ . The middle and bottom panels display, severally, the evolution of the breather's integral power and the evolution of the peak power at  $x = 0$ .

### B. The case of the cubic self-focusing ( $\sigma = 1, \alpha \leq 1$ )

Examples of stable pinned solitons produced by the numerical solution of Eq. (13) with  $\sigma = 1$  and two values of LI,  $\alpha = 1$  and  $0.8$ , are plotted in Fig. 6, along with their VA-produced counterparts. Similar to the examples displayed above for  $\sigma = 2$  (the quintic self-focusing) in Fig. 1, it is seen that the VA produces accurate results.

The results for the existence and stability of the pinned-soliton families under the action of the cubic self-focusing are summarized, by dint of  $P(k)$  curves for two LI values,  $\alpha = 1$  and  $0.8$ , in Fig. 7, cf. Fig. 2 for the case of the quintic self-focusing. In particular, for the critical LI value,  $\alpha = 1$ , the family is completely stable, similar to the complete stability of the pinned-soliton family for the critical value  $\alpha = 2$  in the quintic model [24]. Further, for  $\alpha < 1$  the instability boundary is again determined by the VK criterion, coinciding with the point of  $dP/dk = 0$ . Also similar to the quintic model, in the cubic one the VA accuracy

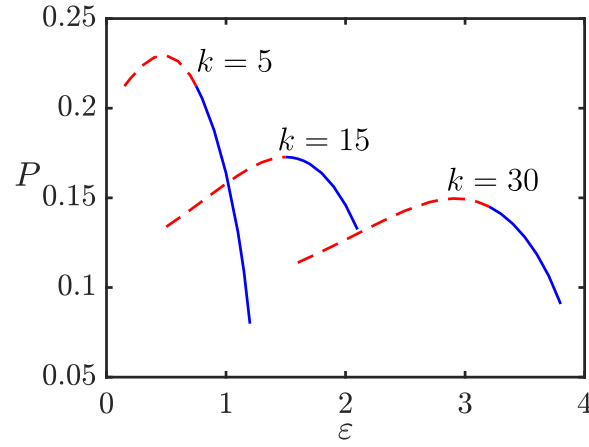


FIG. 5. Numerically produced  $P(\varepsilon)$  dependences for the solitons pinned to the potential  $U(x) = -\varepsilon\tilde{\delta}(x)$ , for the quintic self-focusing ( $\sigma = 2$ ) and  $\alpha = 1$  in Eqs. (12) and (13)), with fixed values of  $k$ , as indicated in the figure (recall that, unlike the case of  $\alpha \neq 1$ , the strength of the attractive  $\delta$ -functional potential cannot be scaled to be  $\varepsilon = 1$  in the case of  $\alpha = 1$ ). Solid blue and dashed red segments designate stable and unstable pinned solitons, respectively.

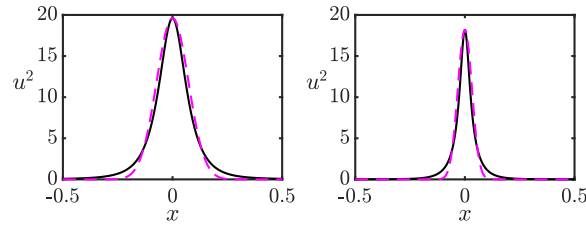


FIG. 6. Power profiles,  $(u(x))^2$ , of the numerically found and VA-predicted stable solitons are displayed by continuous black and dashed magenta lines, respectively, in the case of the cubic self-focusing ( $\sigma = 1$ ) and propagation constant  $k = 13$  in Eq. (13). The corresponding LI values  $\alpha$  are indicated in panels. The solitons are pinned to potential  $U(x) = -\tilde{\delta}(x)$ , see Eq. (14).

improves with the decrease of LI (which is the case of the main interest), making VA quite accurate for  $\alpha = 0.8$ .

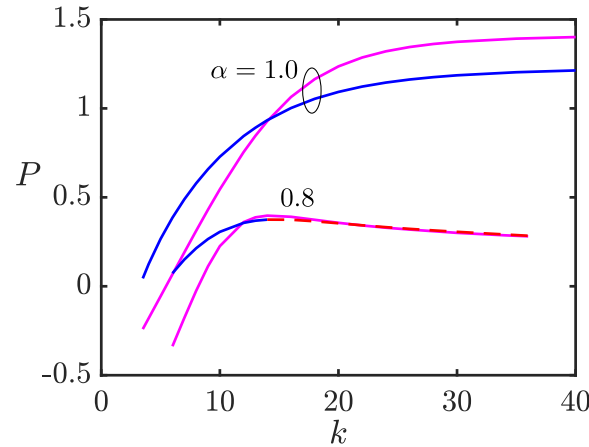


FIG. 7. The power,  $P$ , of families of the fractional solitons pinned by the attractive potential  $-\tilde{\delta}(x)$ , vs. the propagation constant,  $k$ , for the cubic nonlinearity ( $\sigma = 1$ ) and LI values  $\alpha$  indicated in the figure. Solid blue and dashed red lines designate stable and unstable solitons, respectively. The VA-predicted soliton families, produced by the numerical solution of Eqs. (20) and (21), are plotted by solid magenta lines.

The evolution of unstable pinned solitons under the action of the cubic self-focusing term is qualitatively similar to that displayed above in Fig. 4 in the case of the quintic nonlinearity, i.e., spontaneous rearrangement into robust breathers, as demonstrated by the typical example which is presented in Fig. 8 for  $\sigma = 1$  and  $\alpha = 0.8$ . On the other hand, it is seen in the figure that in the present case, unlike the one presented in Fig. 4, the inner oscillations of the breather are almost regular.



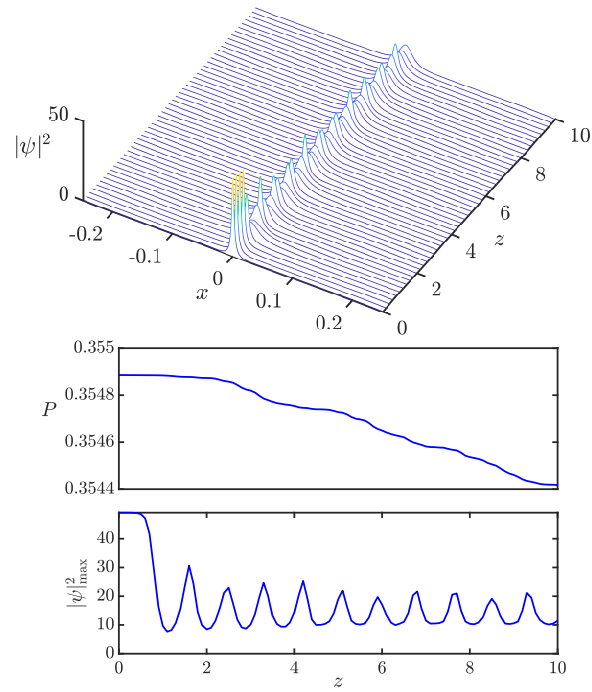


FIG. 8. The top panel: spontaneous transformation of an unstable pinned soliton, with propagation constant  $k = 20$ , into a breather, produced by simulations of Eq. (12) with  $\sigma = 1$  and  $\alpha = 0.8$ . The middle and bottom panels display, severally, extremely slow decay of the breather's integral power due to very weak emission of radiation, and the evolution of the peak power, at  $x = 0$ .

As mentioned above, the LI value  $\alpha = 1$  requires additional consideration, as in this case the strength of the delta-functional attractive potential cannot be fixed as  $\varepsilon = 1$  by means of rescaling. For this case, properties of the pinned-soliton families are summarized in Fig. 9 by means of  $P(\varepsilon)$  curves for three fixed values of the propagation constant,  $k = 5, 15$ , and  $30$ . The comparison with the similar plot for the model with the quintic nonlinearity, which is presented above in Fig. 5, demonstrates that the stability area is larger in the case of the cubic self-focusing. This is a natural conclusion, as the lower-order nonlinearity implies a weaker drive for the instability.

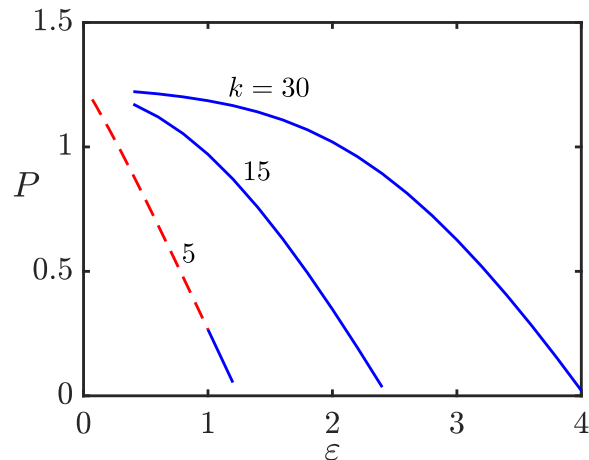


FIG. 9. Numerically produced  $P(\varepsilon)$  dependences for the solitons pinned to the potential  $U(x) = -\varepsilon\delta(x)$  in the case of the cubic self-focusing ( $\sigma = 1$ ) and  $\alpha = 1$  in Eqs. (12) and (13)), with fixed values of  $k$ , as indicated in the figure (recall that, unlike the case of  $\alpha \neq 1$ , the strength of the attractive  $\delta$ -functional potential cannot be scaled to be  $\varepsilon = 1$  in the case of  $\alpha = 1$ ). Solid blue and dashed red segment designate stable and unstable pinned solitons, respectively.

## IV. THE INTERACTION OF A FREE SOLITON AND SOLITON PAIR WITH ATTRACTIVE AND REPULSIVE DEFECTS

### A. Collision of a moving soliton with the attractive or repulsive defect

In the framework of the interaction of fractional solitons with local potentials, another relevant problem is collisions of moving solitons (in fact, tilted ones, in the spatial domain in optics) with attractive and repulsive defects, in the case of the cubic FNLSE ( $\sigma = 1$ ) with  $\alpha > 1$ , as in this case the solitons are stable and may move in the free space, even though FNLSE is not a Galilean-invariant equation [9]. To this end, we address Eq. (12) with  $\sigma = 1$ , written as

$$i\frac{\partial\psi}{\partial z} = \frac{1}{2} \left( -\frac{\partial^2}{\partial x^2} \right)^{\alpha/2} \psi - |\psi|^2 \psi \mp \tilde{\delta}(x) \psi, \quad (28)$$

with the bottom sign (+) in front of  $\tilde{\delta}(x)$  corresponding to the repulsive defect, unlike the attractive one considered above. The regularized delta function in Eq. (28) is taken as per Eq. (14).

Far from  $x = 0$ , the moving soliton is sought for as

$$\psi(x,z) = e^{ikz} u(X), \quad X \equiv x - cz, \quad (29)$$

where  $k$  is the propagation constant, and  $c$  is the "velocity" (actually, it is the tilt of the soliton's trajectory in the spatial domain), and function  $u(X)$  is complex, unlike real  $u(x)$  in Eq. (3). The substitution of ansatz (29) in Eq. (28) yields, far from the defect, the stationary equation in the moving reference frame:

$$ku + ic\frac{du}{dX} + \frac{1}{2} \left( -\frac{d^2}{dX^2} \right)^{\alpha/2} u - |u|^2 u = 0, \quad (30)$$

cf. Eq. (13). Numerical solutions of Eq. (30) are obtained by separating its real and imaginary parts and solving the resulting equations in the moving reference frame. The instantaneous coordinate of the soliton's center is  $X_0 = 5$  of its center

its real and instantaneous

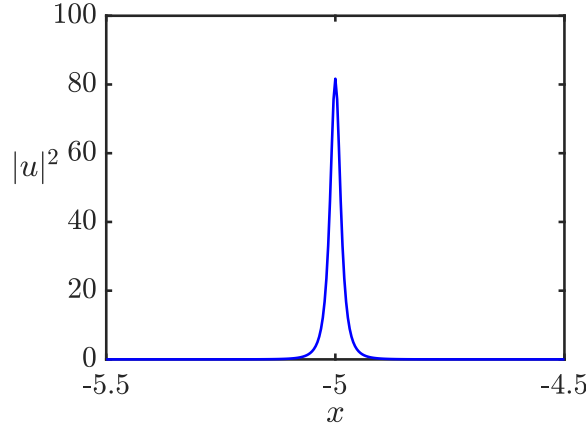


FIG. 10. A typical profile of a stable narrow "moving" (tilted) soliton, produced by the numerical solution of Eq. (30) with  $\alpha = 1.2$ ,  $c = 0.5$ , and  $k = 30$ . The instantaneous coordinate of the soliton's center is  $X_0 = -5$ .

As shown in Fig. 11, the collision of the incident soliton with the repulsive defect naturally leads to rebound with velocity  $-c$ , if  $c$  is smaller than a threshold value, which is  $c_{\text{thr}} \approx 0.55$  for the soliton with  $\alpha = 1.2$  and  $k = 30$  in Eq. (30). The evolution of the soliton's peak power, which is plotted in the bottom panel of Fig. 11, demonstrates that the rebound is not fully elastic, as a part of the power is lost with radiation emitted in the course of the collision.

Further, in the interval of the incidence velocity  $0.55 < c < 0.72$  the collision with the repulsive defect leads to splitting of the incident soliton into passing and bouncing ones, as shown in Fig. 12 for  $c = 0.625$ . Finally, at  $c > 0.75$  the moving soliton passes through the repulsive defect without a velocity loss. An example of the latter outcome is presented in Fig. 13 for  $c = 0.82$ .

Finally, the incident soliton with any velocity readily passes the attractive defect, An example is shown in Fig. 14 for a slow soliton, with velocity  $c = 0.1$ . The evolution of the soliton's peak power, plotted in the bottom panel, demonstrates that the collision is not fully elastic, as it causes excitation of an intrinsic mode in the soliton.

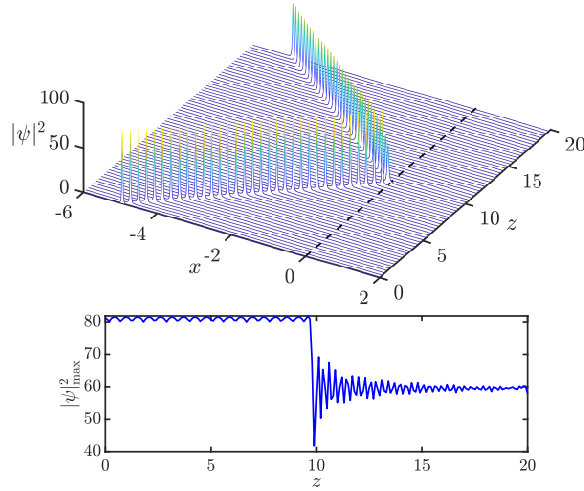


FIG. 11. The rebound of the incident soliton, with parameters  $\alpha = 1.2$ ,  $k = 30$ , and  $c = 0.5$ , from the repulsive defect, as produced by simulations of Eq. (28) with sign + in front of the delta-function. The bottom panel shows the evolution of the soliton's peak power.

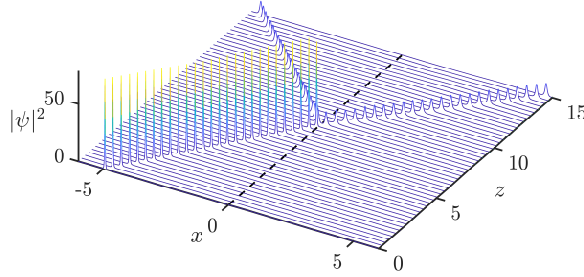


FIG. 12. The splitting of the soliton colliding with the repulsive defect, produced by simulations of Eq. (28) with sign + in front of the delta-function. The parameters are  $\alpha = 1.2$ ,  $k = 30$ , and  $c = 0.625$ .

### B. A two-soliton stationary state pinned to a repulsive defect

In the case of the normal (non-fractional) diffraction,  $\alpha = 2$ , Eq. (13) with the general nonlinearity degree,  $\sigma$ , and repulsive delta-functional potential ( $\varepsilon < 0$ ), admits an exact solution in the form of a bound state of two solitons with propagation constant  $k > |\varepsilon|/\sqrt{2}$  and centers placed at points  $x = \pm x_0$ :

$$\Psi_{\text{two-sol}}(x, z) = \left[ \sqrt{(\sigma + 1)k} \operatorname{sech}(\sqrt{2k}(|x| - x_0)) \right]^{1/\sigma} e^{ikz}, \quad (31)$$

$$x_0 = \frac{1}{2\sigma\sqrt{2k}} \ln \left( \frac{\sqrt{2k} + |\varepsilon|}{\sqrt{2k} - |\varepsilon|} \right). \quad (32)$$

Roughly speaking, this bound state exists due to the balance between the repulsive force exerted by the defect on the solitons, and mutual attraction between the partly overlapping in-phase solitons. However, unlike the formally similar exact solution for the single soliton pinned to the attractive defect, which is given by Eqs. (7) and (11), the two-soliton bound state is unstable, as it is pinned to the repulsive potential center.

It may be interesting to consider a similar bound state in the framework of FNLSE (28) with the cubic self-focusing ( $\sigma = 1$ ), LI  $\alpha > 1$ , and sign + in front of  $\tilde{\delta}(x)$ . The numerical solution demonstrates that such states indeed exist, but are unstable against splitting into free separating solitons, with spontaneous breaking of the symmetry between them. A typical example is shown in Fig. 15 for  $\alpha = 1.5$  and  $k = 0.8$ .

## V. CONCLUSION

Currently, much interest is drawn to theoretical investigations and experimental realizations of nonlinear physical media with effective fractional diffraction, characterized by the respective value of the LI (Lévy index)  $\alpha$ . The usual (non-fractional)

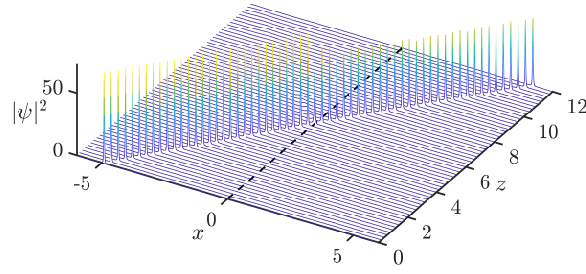


FIG. 13. The fast soliton passing through the repulsive defect, with parameters  $\alpha = 1.2$ ,  $k = 30$ , and  $c = 0.82$ . The picture is produced by simulations of Eq. (28) with sign + in front of the delta-function.

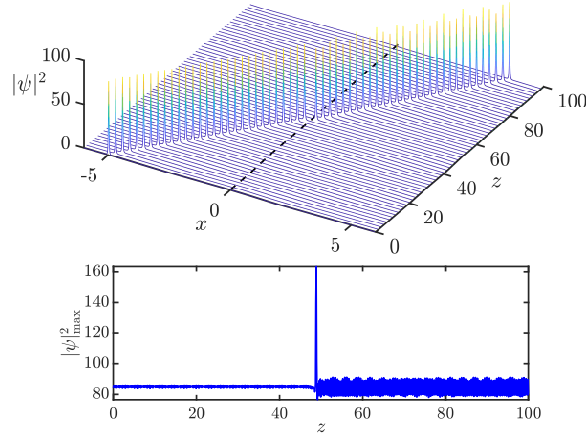


FIG. 14. The soliton with  $\alpha = 1.2$ ,  $k = 30$ , and  $c = 0.1$  passing the attractive defect. The bottom panel demonstrates that the collision leads to excitation of a small-amplitude intrinsic mode in the incident soliton. The picture is produced by simulations of Eq. (28) with sign – in front of the delta-function.

diffraction corresponds to  $\alpha = 2$ , while the nontrivial region is  $\alpha < 2$ . In particular, fractional solitons and other nonlinear modes are promising objects for the realization in optics. In this context, an important problem is the stability of fractional solitons, as, in the free 1D space, they are completely unstable in the case of the cubic self-focusing and  $\alpha \leq 1$ . Furthermore, in the case of the quintic self-focusing in the free space, which also occurs in nonlinear optics, 1D solitons are unstable at all possible values of LI,  $\alpha \leq 2$ . In this work, we have proposed a possibility to stabilize the 1D fractional solitons by pinning them to the attractive defect, which is represented by the regularized delta-functional potential, in the framework of the corresponding FNLSE (fractional nonlinear Schrödinger equation). This setting is relevant for the creation and potential use of new species of fractional optical solitons. We have demonstrated that the fractional solitons with the cubic self-focusing and  $\alpha = 1$  are made completely stable by the pinning to the attractive defect. The partial stabilization for  $\alpha < 1$  is identified too. Similarly, the previously known fact of the complete stabilization of the usual (non-fractal) solitons by the attractive defect in the 1D medium with the quintic self-focusing and  $\alpha = 2$  is extended by the identification of the stability region for  $\alpha < 2$ . In all cases, the instability boundary is exactly determined by the VK (Vakhitov-Kolokolov) criterion. In addition to the systematic numerical analysis, the semi-analytical VA (variational approximation) is developed. A noteworthy finding is that the VA becomes quite accurate for lower LI values, such as  $\alpha = 1.1$  and  $0.8$  for the quintic and cubic self-focusing, respectively, which correspond to stronger fractionality. Collisions of freely moving stable solitons in the cubic medium with the repulsive and attractive defects are considered too, by means of systematic simulations. The increase of the collision velocity leads to the transition of the outcome of the collisions with the repulsive defect from rebound to splitting and, eventually, to passage.

As an extension of the work, it may be interesting to consider the interplay of the fractional diffraction, self-focusing, and a potential cage (cavity) defined by a pair of repulsive defects. In particular, it may be interesting to consider shuttle motion of a stable soliton trapped in the cage.

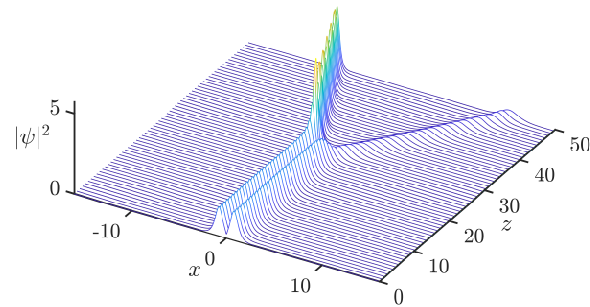


FIG. 15. The symmetry-breaking evolution of the unstable two-soliton bound state pinned to the repulsive defect, with parameters  $\sigma = 1$ ,  $\alpha = 1.5$ , and  $k = 0.8$ . The picture is produced by simulations of Eq. (28) with sign + in front of the delta-function.

#### ACKNOWLEDGMENT

The work of B.A.M. was supported, in part, by the Israel Science Foundation through grant No. 1695/22.

- 
- [1] A. I. Saichev and G. M. Zaslavsky, Fractional kinetic equations: Solutions and applications,” *Chaos* **7**, 753–764 (1997).
- [2] G. M. Zaslavsky, Chaos, fractional kinetics, and anomalous transport, *Phys. Rep.* **371**, 461–580 (2002).
- [3] N. Laskin, Fractional quantum mechanics and Lévy path integrals, *Phys. Lett. A* **268**, 298–305 (2000).
- [4] B. A. Stickler, Potential condensed-matter realization of space-fractional quantum mechanics: The one-dimensional Lévy crystal, *Phys. Rev. E* **88**, 012120 (2013).
- [5] F. Pinsker, W. Bao, Y. Zhang, H. Ohadi, A. Dreismann, and J. J. Baumberg, Fractional quantum mechanics in polariton condensates with velocity-dependent mass, *Phys. Rev. B* **92**, 195310 (2015).
- [6] N. Laskin, *Fractional Quantum Mechanics* (World Scientific, Singapore, 2018).
- [7] S. Longhi, Fractional Schrödinger equation in optics, *Opt. Lett.* **40**, 1117–1120 (2015).
- [8] B. A. Malomed, Optical solitons and vortices in fractional media: A mini-review of recent results, *Photonics* **8**, 353 (2021).
- [9] B. A. Malomed, Basic fractional nonlinear-wave models and solitons, *Chaos* **34**, 022102 (2024).
- [10] S. Liu, Y. Zhang, B. A. Malomed, and E. Karimi, Experimental realisations of the fractional Schrödinger equation in the temporal domain, *Nature Comm.* **14**, 222 (2023).
- [11] S. Secchi and M. Squassina, Soliton dynamics for fractional Schrödinger equations, *Applicable Analysis* **93**, 1702–1729 (2014).
- [12] L. W. Dong, C. M. Huang, and W. Qi, Nonlocal solitons in fractional dimensions, *Opt. Lett.* **44**, 4917–4920 (2019).
- [13] L. Zeng, M. R. Belić, D. Mihalache, J. Li, D. Xiang, X. Zeng, and X. Zhu, Solitons in a coupled system of fractional nonlinear Schrödinger equations. *Physica D* **456**, 133924 (2023).
- [14] S. Liu, Y. Zhang, S. Virally, E. Karimi, B. A. Malomed, and D. V. Seletskiy, Observation of the spectral bifurcation in the fractional nonlinear Schrödinger equation, *Laser & Phot. Rev.* **2025**, 2401714 (2025).
- [15] V. T. Hoang, J. Widjaja, Y. L. Qiang, A. F. J. Runge, and C. M. de Sterke, Observation of fractional evolution in nonlinear optics , arXiv:2410.23671.
- [16] B. B. Mandelbrot, *The Fractal Geometry of Nature* (W. H. Freeman, New York, 1982).
- [17] M. Cai and C. P. Li, On Riesz derivative, *Fract. Calc. Appl. Anal.* **22**, 287–301 (2019).
- [18] M. Caputo, Linear model of dissipation whose Q is almost frequency independent. II,” *Geophys. J. Int.* **13**, 529–539 (1967).
- [19] N. G. Vakhitov and A. A. Kolokolov, Stationary solutions of the wave equation in a medium with nonlinearity saturation, *Radiophys. Quantum Electron.* **16**, 783–789 (1973).
- [20] L. Bergé, Wave collapse in physics: Principles and applications to light and plasma waves, *Phys. Rep.* **303**, 259–370 (1998).
- [21] G. Fibich, *The Nonlinear Schrödinger Equation: Singular Solutions and Optical Collapse* (Springer, Heidelberg, 2015).
- [22] M. Chen, S. Zeng, D. Lu, W. Hu, and Q. Guo, Optical solitons, self-focusing, and wave collapse in a space-fractional Schrödinger equation with a Kerr-type nonlinearity, *Phys. Rev. E* **98**, 022211 (2018).
- [23] F. Kh. Abdullaev and M. Salerno, Gap-Townes solitons and localized excitations in low-dimensional Bose-Einstein condensates in optical lattices, *Phys. Rev. A* **72**, 033617 (2005).
- [24] L. Wang, B. A. Malomed, and Z. Yan, Attraction centers and  $\mathcal{PT}$ -symmetric delta-functional dipoles in critical and supercritical self-focusing media, *Phys. Rev. E* **99**, 052206 (2019).
- [25] A. S. Reyna and C. B. de Araújo, Spatial phase modulation due to quintic and septic nonlinearities in metal colloids, *Opt. Exp.* **22**, 22456 (2014).
- [26] A. S. Reyna and C. B. de Araújo, High-order optical nonlinearities in plasmonic nanocomposites – a review, *Advances in Optics and Photonics.* **9**, 720-774 (2017).
- [27] C. M. Huang and L. W. Dong, Gap solitons in the nonlinear fractional Schrödinger equation with an optical lattice, *Opt. Lett.* **41**, 5636-5639 (2016).

- [28] L. Zeng and J. Zeng, One-dimensional solitons in fractional Schrödinger equation with a spatially periodical modulated nonlinearity: nonlinear lattice. *Optics Letters* **44**, 2661-2664 (2019).
- [29] L. Zeng and J. Zeng, Preventing critical collapse of higher-order solitons by tailoring unconventional optical diffraction and nonlinearities, *Communications Physics* **3**, 26 (2020).
- [30] X. Zhu, M. R. Belić, D. Mihalache, D. Xiang, and L. Zeng, Two-dimensional gap solitons supported by a parity-time-symmetric optical lattice with saturable nonlinearity and fractional-order diffraction, *Optics and Laser Technology* **184**, 112426 (2025).
- [31] S. K. Turitsyn, J. E. Prilepsky, S. T. Le, S. Wahls, L. L. Frumin, M. Kamalian, and S. A. Derevyanko, Nonlinear Fourier transform for optical data processing and transmission: advances and perspectives. *Optica* **4**, 307-322 (2017).
- [32] S. I. Muslih, O. P. Agrawal, and D. Baleanu, A Fractional Schrödinger equation and its solution. *Int. J. Theor. Phys.* **49**, 1746-1752 (2010).
- [33] J. Yang, *Nonlinear Waves in Integrable and Nonintegrable Systems* (SIAM, Philadelphia, 2010).